Cluster Phases of Decorated Micellar Solutions with Macrocyclic Ligands

S. Marchetti,[†] E. Fratini,[‡] S. Sennato,[§] G. Cazzolli,[||] B. Rossi,[||] S. Caponi,[⊥] L. Lanzi,[†] M. Carlà,[†] F. Sciortino,[§] G. Viliani,[||] and C. M. C. Gambi*,[†]

[†]Department of Physics and Astronomy, University of Florence, and CNISM, Via G. Sansone 1, 50019, Sesto Fiorentino, Florence, Italy

[‡]Department of Chemistry and CSGI, University of Florence, Via della Lastruccia 3, 50019, Sesto Fiorentino, Florence, Italy

[§]Department of Physics, Sapienza University of Rome, and CNR-IPCF, Piazzale A. Moro 5, 00185, Rome, Italy

[||]Physics Department, University of Trento, 38123, Povo, Trento, Italy

[⊥]Istituto di Biofisica, Consiglio Nazionale delle Ricerche, Via alla Cascata, 56/C, 38123, Trento, Italy

ABSTRACT: An aqueous self-assembled micellar system (sodium dodecyl sulfate, SDS, decorated with various adhesive sites, cryptand Kryptofix 222 and crown ether 18-Crown-6 molecules) has been investigated by dynamic light scattering (DLS) and small angle x-ray scattering (SAXS) to have insights into the micellar structure, the micellar interactions, and the aggregation properties of the system. DLS demonstrates the existence of populations of aggregates in the submicrometer/micrometer range, while the Guinier analysis of the SAXS curves helps in detailing objects smaller than 30 nm. The aggregates of micelles are here named cluster phases of micelles (CPMs). Considering that SDS micelles in water do not aggregate at low concentration, it is shown that macrocyclic ligands induce the SDS micelle aggregation as a function of the concentration (i.e., investigated ligand/SDS molar ratios are 5.0, 1.5, 1.0, and 0.5) and hydrophobicity of the adhesive sites. The sizes and the percentages of the micelles and the CPMs have been monitored to test the stability and reversibility of the system. DLS results clearly show that the aggregation processes of the decorated micelles are reproducible at time intervals of the order of 1 month, while the stability may not be entirely maintained after a year. As an issue of particular relevance, the higher the ligand/surfactant molar ratio, the larger are the CPMs induced. The K222 ligand results in being more effective in promoting the micellar aggregation than 18C6 as a consequence of the different hydrophobicity.
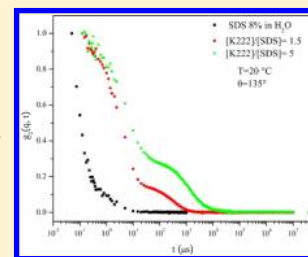
INTRODUCTION

Aggregation processes are an important subject of current research in liquid state physics because understanding the aggregation mechanisms makes it possible to build up new "responsive" materials and to solve important challenges in medicine/biology as well as in several industrial-manufacturing processes. Self-assembly leads to ordered structures like lipid bilayers and proteins in the biophysical field as well as to complex fluids, molecular crystals, polymers, and nanostructures in the material science field.

In this paper, we investigate cluster phases of micelles (CPMs) built up by sodium dodecyl sulfate (SDS) at a concentration of 8% w/w in water and decorated with the macrocyclic ligands Kryptofix 222 (K222) or 18-Crown-6 (18C6) crown ether, to understand the interactions that lead to the aggregation process of decorated micelles in solution. The 8% w/w concentration value was chosen to avoid aggregation between naked SDS micelles. The aggregation processes, we refer to, are at two different levels: the one related to the micellar structure and the other to CPMs.

The ligands are neutral organic molecules that in the micellar solution are able to selectively form stable noncovalent host/guest complexes[1] enclosing some of the sodium counterions of the Gouy−Chapman layer[2,3] and to migrate to the micellar surface reducing the charge of the micelles as reported in the literature.[4−8]

The SDS micelles without ligands interact by hard-sphere and screened Coulomb repulsive interactions, whereas the SDS micelles with ligands can be considered "colloidal molecules" or "patchy colloids",[9] i.e., particles decorated on their surface with a well-defined number of adhesive sites (the ligand molecules in our case) that can link to similar sites on other micelles, giving rise to cluster formation.

The cluster phase formation has been observed in globular protein solutions in salt-free conditions as a result of the competition between a long-range screened Coulomb repulsion and a short-range attraction,[10−14] in concentrated protein solutions at different pH and salt concentrations,[11,15] and in concentrated protein solutions and colloids[16] as well as in gelation.[17] In these cases, bulk aggregation is disfavored and finite-size clusters are formed and could persist in equilibrium. In particular, equilibrium cluster phases with low volume fraction are reported in the literature.[18−21]

Previous studies have shown that the ultimate driving force that leads to the formation of CPMs is the hydrophobicity of K222 or 18C6 adhesive sites. In fact, the analysis of electrocapillary curves[5] has demonstrated that K222 ligands strongly adsorb at the mercury–water interface even in the presence of an intermolecular repulsive electrostatic contribution due to Na^+ cations trapped inside the macrocyclic cages.

Since the 1980s, it has been known that SDS molecules in conditions similar to those investigated in this work, namely, at concentration C = 0.25 M and temperature T = 25 °C, exhibit self-assembly in uniform-size micelles of spheroidal shape with an aggregation number of the order of 100, charge 30, axial ratio around 1.3, and hydrodynamic diameter of 50 Å.[22,23] Due to the partial ionization of the sulfate groups, each micelle has a negative surface charge and some SO_4^- groups remain unscreened because of the migration of the Na^+ ions into the Gouy–Chapman diffuse layer.[2] The interaction potential between the micelles can be described by the combination of both hard-sphere and screened Coulomb repulsion.[24,25]

Since the 1990s, SDS micelles in water in the presence of macrocyclic ligands K222 or 18C6 were intensively studied by small angle neutron scattering (SANS). According to SANS measurements,[4,6,7] both ligands localize at the micellar surface. It was seen that, as the K222/SDS molar ratio changes from 0.5 to 1.5, the thickness of the polar head region at the SDS micellar interface increases from 5.5 to 10 Å,[26–28] while both the micellar surface charge and the aggregation number decrease. Furthermore, the fraction of interfacial ligands increases from 40 to 65% over the total surfactant molecules. The surface charge is the same as for naked micelles, the aggregation number is 74 as for K222 with molar ratio 0.5, the interfacial amount of ligand is lower (11%), the axial ratio is 1.4, and the diameter of the micelle is 48 Å.

Lithium dodecyl sulfate (LDS) micelles were also studied[4] with addition of 18C6 at the ratio 18C6/LDS = 1.0. The resulting thickness of the polar head is 5.5 Å (the same as for SDS naked micelles), and the ligand does not penetrate into the micellar core, leading to infer that the plane of the crown-ether is tangential to the micellar surface. The crown-ether screening effect for the counterion is smaller than in the cryptand case.

From dielectric spectroscopy measurements,[29–31] three relaxation processes have been found in SDS micellar solutions both with and without complexation with macrocyclic ligands, K222 and 18C6. Two relaxations are of micellar origin, at 30 and 300 MHz, as a result of the radial and lateral motions of the diffuse ion cloud around the micelle; the third relaxation, close to 20 GHz, corresponds to bulk water contribution.[32] The presence of ligands either K222 or 18C6 is seen to deeply alter the dielectric spectra, broadening the micellar contribution, shifting to higher frequencies both micellar relaxations and redistributing their dielectric strengths. The observed changes have been attributed to a reorganization of the system, where the ligand-decorated micelles aggregate in large clusters, as a result of the progressive reduction of both the surface charge and thickness. These findings suggest the possibility to tune the aggregation of the decorated micelles by finely controlling the amount of complexed ligand at the micellar surface.

Raman scattering experiments and numerical simulations have been used to obtain more information on the micellar aggregation process.[33] Raman spectra of SDS micellar solutions both pure and decorated with various adhesive sites have been compared in order to identify specific bands sensitive to the aggregation process. The numerical simulation helped the assignment of these bands. The comparison of the spectra shows differences in intensity and wavenumber, confirming the sensitivity of the Raman spectroscopy to the aggregation process and the ability of this technique to characterize the CPMs.

While it is well-known that SDS micelles in water do not aggregate, in this work, we give experimental evidence by dynamic light scattering (DLS) and small angle X-ray scattering (SAXS) that it is possible to induce aggregation by decorating the SDS micellar surface with macrocyclic ligands. Furthermore, the aggregation can be tuned by changing the ligand/surfactant ratio and the hydrophobicity of the ligand.

■ SAMPLES PREPARATION AND CHARACTERIZATION

Aqueous solutions of 8% w/w SDS/(SDS + water) and (SDS + ligand)/(SDS + ligand + water) were prepared at different ligand/SDS molar ratios. SDS with 99% purity was purchased from Aldrich, while the ligands Kryptofix 222 and 18-Crown-6 were from Merck. All the products were used as received.

The SDS density is 1.01 $g\,cm^{-3}$, and the CMC (critical micellar concentration) in water is 8.1 mM^{34} at 25 °C. The density of K222 and 18C6 molecules is 1.11 and 1.10 $g\,cm^{-3}$, respectively. The SDS solutions with K222 and 18C6 at 25 °C have, respectively, CMC = 1.6^{22} and 7.1 mM.[35]

The hydrophobicity of the two ligand molecules, according to the common definition,[36] has been determined calculating the $\log_{10}(P)$, where P is the partition coefficient in n-octanol/water. $\log_{10}(P)$ was calculated using the ChemProp module in the ChemDraw Suite, v.11,[37] which implements the fragmentation approaches by Crippen[38] and Broto.[39] The values extracted using these two procedures show a lower $\log_{10}(P)$ for the K222 ligand (−1.18 and −1.72) compared to the 18C6 ligand (−0.93 and −0.49), thus evidencing a slightly higher hydrophobicity for the latter molecule. According to the reported values, both ligands show a slightly higher affinity to water than to the organic phase.

SDS solutions in water and SDS solutions with ligand in water were filtered with 0.45 μm pore size Millipore filters in order to have dust free solutions. Millex-HV (PVDF), Millex LCR, and PTFE filters were used. One solution was centrifuged to remove dust using a Beckman J2-21 centrifuge, with 3100 rpm for 2 h. The samples were the same for both methods, filters or centrifuge. The micellar solutions were prepared in cylindrical light scattering cells (2.5 cm inner diameter). All the samples were transparent, and homogeneous. We verified that no liquid crystal structure was present in the samples.

The index of refraction for K222 and 18C6 micellar solutions at 20 °C was measured with an Abbe refractometer (ATAGO 3T) with a resolution of 0.0001 at 550 nm. Obtained values are reported in Table 1. The index of refraction for the 18C6/SDS = 1.0 and K222/SDS = 1.5 solutions for some temperatures in the range 25−40 °C is reported in Table 2. All the samples were thermally stabilized by means of a thermostat with an accuracy of ±0.2 °C.

■ METHODS

Dynamic Light Scattering. DLS experiments were carried out on a Brookhaven Instruments apparatus (BI 9000AT correlator and BI 200 SM goniometer). The signal was detected with an EMI 9863B/350 photomultiplier. The light source was a Coherent Verdi V2 laser at the wavelength 532 nm, with the

Table 1. Index of Refraction n at the Wavelength 550 nm for Solutions of Micelles Decorated by K222 or 18C6 Ligands at 20 °C

solution	n
K222/SDS	
5.0	1.3984
1.5	1.3635
18C6/SDS	
1.5	1.3562
1.0	1.3509
0.5	1.3466

Table 2. Index of Refraction n at the Wavelength 550 nm for Solutions of Micelles Decorated by K222 or 18C6 at Incremental Temperatures from 25 to 40 °C

	n	
T (°C)	18C6/SDS = 1.0	K222/SDS = 1.5
25	1.3509	1.3624
30	1.3504	1.3616
35	1.3486	1.3603
40	1.3478	1.3596

beam linearly polarized in the vertical direction and conveniently attenuated in order to avoid sample heating (maximum power 100 mW). The long-term power stability of the laser was ±0.5%. The scattering angle θ (i.e., the angle between the direction of forward propagation and the direction along which the scattered light is collected) was measured using a goniometer with a resolution of 0.01°. Homodyne detection[40] was recorded in the angular range 15−155°.

The measuring cell was immersed in decahydronaphthalene as a matching liquid. To calibrate the apparatus, a solution of 94 nm diameter latex spheres from SERVA, Standard Dow Latex, was used in the angular range 15−155°. The data analysis of the latex solution was performed by cumulant expansion considering only up to the second moment.[28]

In the DLS technique, the measured quantity is the normalized time autocorrelation function $g_2(q, t)$ of the scattered light intensity $I(q, t)$ defined by

$$g_2(q, t) = \frac{\langle I(q, 0) \times I(q, t) \rangle}{\langle I(q, 0)^2 \rangle} \tag{1}$$

where t is the time and $q = (4\pi n/\lambda) \sin(\theta/2)$ is the modulus of the scattering wave vector, with n being the refractive index of the sample and θ the scattering angle. In turn, $g_2(q, t)$ can be expressed in terms of the normalized electric field autocorrelation function $g_1(q, t)$ through the Siegert equation:[28]

$$g_2(q, t) = A\{1 + \beta[g_1(q, t)]^2\} \tag{2}$$

where A is the measured baseline and β is the spatial coherence factor.[28] For a dilute suspension of monodisperse particles, $g_1(q, t)$ decays exponentially with a decay rate of $\Gamma = Dq^2$, where D is the translational diffusion coefficient, which is related to the hydrodynamic diameter $d = 2R_H$ (where R_H is the hydrodynamic radius of the particle; the latter is somewhat larger than the true radius because of some water molecules attached to the micelles and CPMs) through the Stokes−Einstein relationship $D = K_B T/(6\pi \eta R_H)$, with $K_B T$ the thermal energy and η the viscosity of the aqueous phase. In the case of polydisperse samples, $g_1(q, t)$ deviates from a single exponential

decay and can be written as the Laplace transform of a continuous distribution $G(\Gamma)$ of decay times:

$$g_1(q, t) = \int_0^\infty G(\Gamma) e^{-\Gamma t} \, d\Gamma \tag{3}$$

The analysis of the decay time distribution has been performed with the inverse Laplace transform by means of the CONTIN routine, a commonly employed constrained regularization method.[28,41]

Small Angle X-ray Scattering. SAXS measurements were carried out with a Rigaku Nanoviewer instrument equipped with a mercury charge coupled device detector containing 1024 × 1024 pixels of width 68 μm. Cu Kα radiation at a wavelength of 1.542 Å was provided by a Rigaku Micromax007 X-ray rotating anode, operating at a maximum power of 0.8 kW; the source produced a circular focal spot of 70 μm diameter. X-rays were conditioned using the Confocal Max-Flux Mirror (Rigaku/Osmic) to totally remove the Cu Kβ radiation while maintaining the high flux and symmetry of the rotating anode source. X-ray collimation was performed through a three-point collimation system. The sample-to-detector distance was about 605 mm. The volume between the sample and the detector was kept under vacuum during the measurements to minimize the scattering from air. The Q-range was calibrated using silver behenate, which is known to have a well-defined lamellar structure (d-spacing = 58.38 Å).[42] Scattering curves were measured in a Q-range from 0.01 to 0.6 Å^{-1}. The liquid samples were introduced into a 1 mm borosilicate Mark-Tube (Hilgenberg GmbH, Germany) using a syringe. In all cases, the capillary was sealed to avoid sample evaporation. The temperature was controlled with a Peltier element, with an accuracy of ±0.1 °C. All 2-D SAXS patterns were corrected for the dark current, and the Dezinger procedure was applied to remove spurious signals. The solvent/cell contribution (water in borosilicate capillary) was removed using the relative sample/solvent transmissions. Finally, 2-D images were azimuthally averaged to obtain the correspondent 1-D scattering intensity distribution. Data reduction was performed by using Nika and Irena[43] packages. The SAXS scattering lengths of the K222 and 18C6 ligands are 5.8092 × 10^{-5} and 4.0608 × 10^{-5} Å, respectively. The molecular volume is 9.1 Å^3 for sodium ion, 29.9 Å^3 for the water molecule, and 414.6 Å^3 for the SDS molecule. Hence, the resulting scattering length density for the sodium ion is 3.099 × 10^{-5} Å^{-2}, sulfate group 1.8934 × 10^{-5} Å^{-2}, surfactant chain 0.7929 × 10^{-5} Å^{-2}, water 0.94314 × 10^{-5} Å^{-2}, K222 ligand 1.0318 × 10^{-5} Å^{-2}, and 18C6 ligand 7.3526 × 10^{-5} Å^{-2}.

■ RESULTS

DLS and SAXS techniques have been used to characterize the formation of aggregates in CPMs. The DLS analysis allows one to obtain the size of the different particles in solution as well as their contribution to the scattered light. From SAXS analysis, we can extract details on the micellar structure in terms of size, shape, interactions between micelles (Debye's length and contact potential), and volume fraction. Furthermore, the Guinier's law applied to the low Q-range of the SAXS curves allows one to extract the radius of gyration of the CPMs.

Dynamic Light Scattering. For samples with K222 and 18C6 ligands, data processing was performed by the CONTIN analysis mentioned above. As to the SDS sample without ligand, CONTIN analysis showed a single relaxation time; in this case, we preferred to process the data with the cumulant

analysis. The SDS micellar solution without ligand is composed of micelles with a size of 5.6 and 10% polydispersity.

DLS measurements have been made at scattering angles in the range 50−155°. As representative measurements, we report the results at 135°.

Figure 1 shows the autocorrelation functions for the samples with K222/SDS ratios 5.0, 1.5, and 0 (i.e., SDS without ligand).
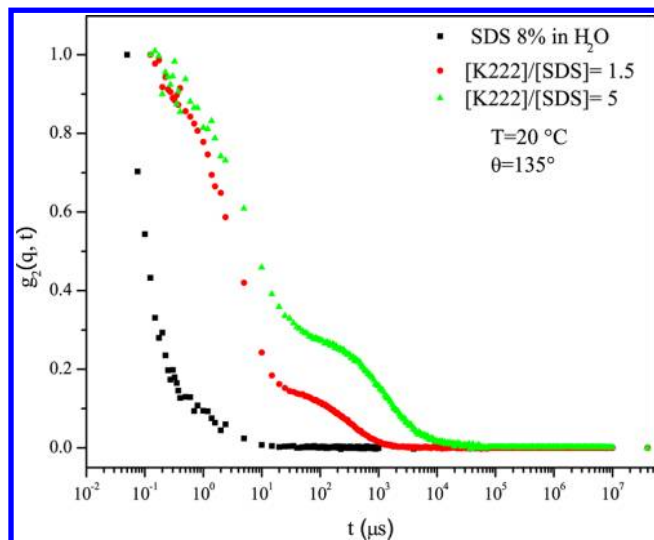

Figure 1. Linear-log autocorrelation functions of the SDS micellar samples decorated by K222 ligand with K222/SDS ratios of 5.0 (green) and 1.5 (red) and of the sample without ligand (black) at 20 °C for the 135° angle.

The curves evidence more than one relaxation time in the case of K222 added samples, whereas only one relaxation time is present when the micellar solution contains no ligand.

In Figure 2, the CONTIN residuals of the sample K222/SDS with ratio 5.0 are reported for the time interval used for the
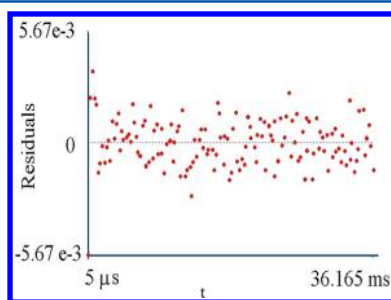

Figure 2. CONTIN residuals of the sample K222/SDS ratio 5.0 (green) shown in Figure 1.

fitting. Their regular distribution accounts for an unbiased quality of the fit. Figure 3 presents the size distribution of the same sample as the percent intensity of the scattered light vs $\log_{10}(d)$, where d is the size of the particles. Two main populations are clearly visible, one in the range 3−5 nm due to the micelles, and the other in the range 500−5000 nm due to large aggregates.

Figure 4 displays in linear-log scale the autocorrelation functions of the SDS micellar solutions in water with 18C6/SDS ratio 1.0 and 1.5, together with the SDS sample without ligand. In comparison with the K222 sample (Figure 1), the
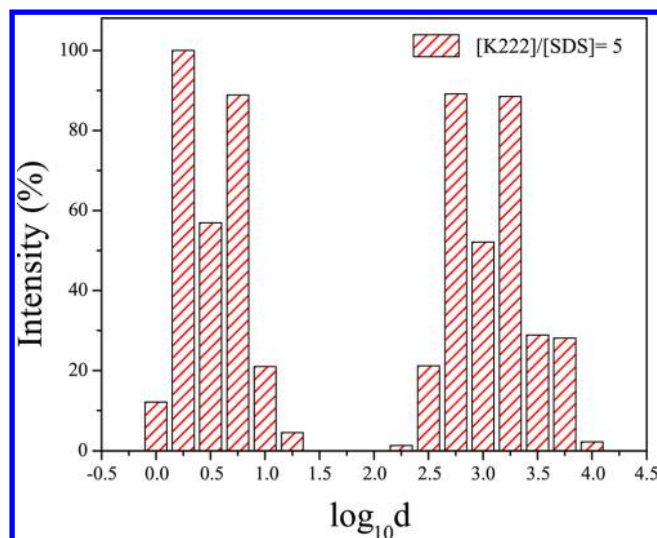

Figure 3. Linear-log histogram of the K222/SDS = 5.0 sample reported as a function of the intensity distribution vs the diameter d.
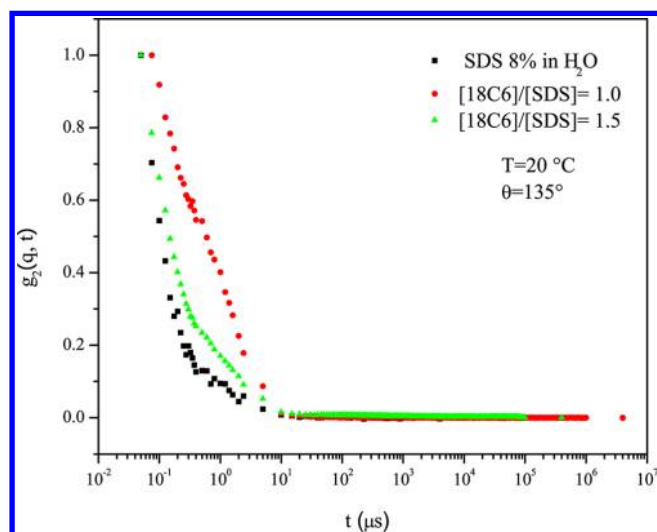

Figure 4. Linear-log autocorrelation functions of the SDS micellar samples decorated by 18C6 ligand with 18C6/SDS ratios of 1.0 (red) and 1.5 (green) at 20° for the angle of 135° and of the SDS sample without ligand (black).

curve features are downscaled to much shorter correlation times.

Figure 5 shows the autocorrelation functions in linear-log scale for the SDS micellar solutions in water with ratio 18C6/SDS = 1.0 for several temperatures in the cycle 20 °C → 30 °C → 40 °C → 20 °C. Apart from a vertical shift of the first curve at 20 °C, the main features appear to be common to all temperatures.

We recall that the intersection temperature of the solubility and the CMC curves is referred to as the Krafft point or temperature (T_K). This temperature, which is characteristic for each surfactant, defines the value below which the surfactant precipitates out of the solution as hydrated crystals. The micelles coexist with the monomer at temperatures higher than given by the solubility curve and concentrations higher than given by the CMC curve.[3] For the SDS/water system, T_K is about 22 °C.[3] Above this temperature, the solubility increases rapidly, whereas cooling below 22 °C, the surfactant solution
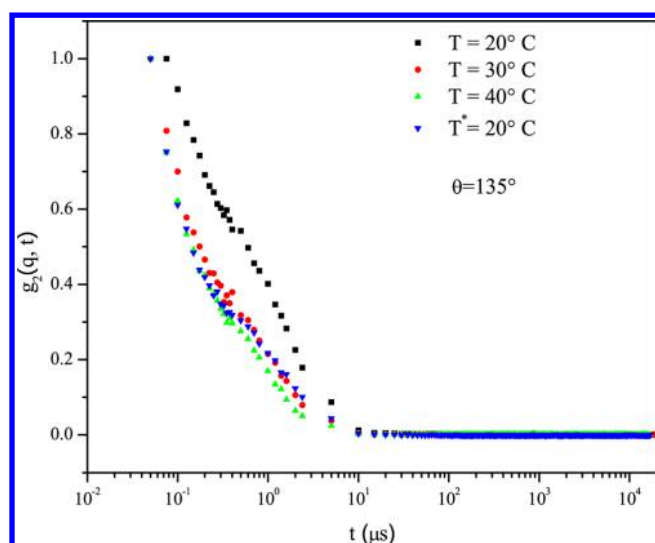
Figure 5. Linear-log autocorrelation functions of the SDS micellar samples decorated by 18C6 ligand with an 18C6/SDS ratio of 1.0 at different temperatures for the angle of 135°.

can remain in a metastable state. In our study, we investigated the temperature range 20−40 °C that includes a small part of the metastable region. Considering this lower limit (i.e., 20 °C) for the SDS/water system, we observed only one relaxation process in the DLS autocorrelation function, suggesting that no significant hydrated crystals are present in this case. On the other hand, for the SDS/K222 and SDS/18-C6 systems, more than one relaxation process is present (see Figures 1, 4, and 5) as a result of the CPM formation.

Detailed results of our measurements are reported in the following tables. The micelle diameter is given as a range, extending from 3 to 5 nm. This is due to the fact that the data are affected by the instrumental response of the detector. As long as the system is linear, the autocorrelation function of the micellar contribution is convoluted with the autocorrelation function of the pulse response of the photomultiplier. Since the latter function is narrower than that of the micelles, the convolution basically reproduces the micellar contribution, only slightly widened.

In Tables 3−7, we report the diameter and the scattered light intensity percentage of the micelles and of the CPMs for all cases we studied. We did not implement deconvolution to work out the micellar contribution from DLS measurements because we used SAXS analysis to extract such information, with the SAXS technique being better suited than DLS to give a detailed structure for the decorated micelles (see below).

In the following subsections, results separately for K222 and 18C6 samples are described.

SDS Samples with K222 at 20 °C. The system was composed of small particles (micelles) and CPMs of significantly larger size. In particular, the micelles had a size of approximately 5 nm, as shown by SANS[7] and SAXS analysis, while the size of CPMs, of the order of micrometers, was distributed over a rather large range. It is known from the diffraction law that larger particles scatter more at smaller angles, and the contrary for smaller particles. This is noticed in Table 3, where the particle size and the percentage of the population (by intensity of the scattered light) obtained by the CONTIN analysis for the SDS sample with ratio K222/SDS = 5.0 is reported at 20 °C in the angular range 150−50°. For example, it is noticed that at $\theta = 90°$ the intensity of the scattered light contains a 23% contribution due to the micelles (3−5 nm size), 2% due to midsize aggregates (20−30 nm), and 75% due to aggregates of size 800−2000 nm; conversely, at $\theta = 135°$, the contribution due to micelles increases to 42%, the contribution of 2% due to midsize aggregates (20−30 nm) is still present, and the remaining contribution (due to aggregates that are distributed in the range 500−5000 nm) decreases to 56%; the detail of the distribution at $\theta = 135°$ has been shown in Figure 3. This system is basically composed of small micelles of 5 nm and CPMs of large size (500−5000 nm) that scatter according to the Rayleigh and Mie law, respectively.[40] The latter produce a diffraction pattern like an antenna with sharp and intense forward lobe.

In order to explore the temporal evolution of the samples, all measurements were repeated at different times. All samples, stored at 4 °C, were stirred and thermally stabilized at room temperature at 20 °C for one night. Routinely, a second measurement was made after 1 month. The results were processed with the CONTIN routine, getting the values reported in the lower part of Table 3. Residuals were lower than 1.5%. The light intensity for the micelles confirmed after the 1 month time interval the decreasing trend from 150 to 50°, whereas the light intensity of the medium CPMs was quite low, and the intensity of the large CPMs accounted for a forward Mie scattering with higher contribution at smaller angles.

In Table 4, the results by CONTIN analysis for the SDS sample with K222/SDS = 1.5 ratio at 20 °C in the angular range 150−50° are reported. The fit residuals are lower than 5%.

The comparison of the SDS samples with ratio K222/SDS = 5.0 (Table 3) and K222/SDS = 1.5 (Table 4) evidences a significant amount of large CPMs in the 5.0 sample and a small amount in the 1.5 sample, whereas the midsize CPMs are very few in the 5.0 sample as compared to those in the 1.5 sample. Thus, the more the K222 ligand is in the sample, the larger the CPMs are in the solution.

In Table 4, the micelle contribution to light intensity at all the scattering angles under investigation is of significance, as well as the contribution due to midsize aggregates. At the extreme scattering angle of $\theta = 50°$, a small contribution due to large size aggregates (5000 nm) is also observed.

Table 4 also includes a section with measurements made after 2 years. The contribution to the scattered light from midsize aggregates increases as the angle varies from $\theta = 150°$

Table 3. Hydrodynamic Diameters for the Micelles and CPMs in the SDS Sample with K222/SDS = 5.0 Ratio at 20 °C in the Angular Range 150−50° and Percentage of Contribution to the Intensity of the Scattered Light

θ (angular deg)	micelles ø (nm)	%	aggreg medium (nm)	%	aggreg large (nm)	%
150	3−5	42	300−500	22	5000	36
135	3−5	42	20−30	2	500−5000	56
90	3−5	23	20−30	2	800−2000	75
50	3−5	8	20−30	1	1200−3000	91
After 1 Month						
150	3−7	56	300−500	21	3000−5000	23
135	3−5	57	20−30	3	500−5000	40
90	3−5	44	20−30	3	500−5000	53
50	3−5	21	20−30	5	1200−5000	74

Table 4. Hydrodynamic Diameters for Micelles and CPMs in the SDS Sample with K222/SDS = 1.5 at 20 °C in the Angular Range 150−50° and Percentage of Contribution to the Intensity of the Scattered Light

θ (angular deg)	micelles ⌀ (nm)	%	aggreg medium (nm)	%	aggreg large (nm)	%
150	3−7	53	120−500	47		
135	3−5	56	120−500	44		
90	3−5	40	200−800	60		
50	3−5	28	200−500	65	5000	7
			After 2 Years			
150	3−5	64	120−200	9	5000	27
135	3−5	78	120−200	11	3000−5000	11
90	3−5	68	200−500	24	3000−5000	8
50	3−5	62	300−500	27	3000−5000	11

to θ = 50°, showing a Mie scattering trend, while for large size aggregates such contribution decreases. This might indicate that samples become less stable over time intervals of the order of years.

K222 Samples at 30−40°. To check the stability and the reversibility of the CPMs as a function of temperature, we performed DLS measurements changing the temperature from 20 to 30 and 40 °C and back to 20 °C.

Results obtained by the CONTIN analysis are reported in Table 5 for the SDS sample with ratio K222/SDS = 1.5 and

Table 5. Hydrodynamic Diameters for Micelles and CPMs of the SDS Sample with Ratio K222/SDS = 1.5 in the Angular Range 150−50° at Different Temperatures

θ (angular deg)	micelles ⌀ (nm)	%	aggreg medium (nm)	%	aggreg large (nm)	%
			At 30 °C			
150	3−5	73	200−500	21	800−2000	6
135	3−5	80	80−120	7	800−1200	13
90	3−5	72	300−500	38		
50	3−5	63	300−500	25	2000−5000	12
			At 40 °C			
150	3−5	82	80	4	500−800	14
135	3−5	90	200−300	8	5000	2
90	3−5	45	200−300	30	5000	25
50	3−5	55	200−300	12	5000	33
			At 20 °C without Stirring			
150	3−5	88	200−300	7	2000−3000	5
135	3−5	93	80−120	7		
90	3−5	72	500−800	22	5000	6
50	3−5	44	300−500	18	5000	38
			At 20 °C with Stirring			
150	3−5	86	300−500	11	5000	3
135	3−7	70	300−500	30		
90	3−5	73	300−500	15	5000	12
50	3−5	46	500−800	30	5000	24

angular range 150−50°. For each increase of temperature from 20 to 30 °C and from 30 to 40 °C, the sample was stirred and measured after 1 night of stabilization. The last measurement at 20 °C was made twice, before and after stirring, with 1 night of stabilization in both cases; the first measurement at 20 °C is the one in Table 4, and had been made at a prior time.

The residuals are lower than 5% at 30 °C and lower than 1% at 40 °C. At 20 °C, the residuals are lower than 3 and 5%, respectively, without and with stirring.

The light intensity from micelles shows a variable behavior from 150 to 50 °C, however constituting a major contribution to light scattering. As to midsize and large CPMs, their contribution appears also variable, anyway representing a minor fraction of the scattered light.

Some inconsistencies were noticed comparing the results at 20 °C before and after stirring, likely due to the mechanical action on the system. Other inconsistencies were also observed comparing the final data at 20 °C with the initial ones (Table 4); these can be attributed to having taken such initial measurements at a far earlier time, and considering the poor stability of the system over long time intervals.

18C6 Samples at 20 °C. In Table 6, we report the size and the percentage of contribution to the intensity of the scattered

Table 6. SDS Samples with 18C6/SDS = 0.5, 1.0, and 1.5 at 20 °C in the Angular Range 150−50°

θ (angular deg)	micelles ⌀ (nm)	%	aggreg medium (nm)	%	aggreg large (nm)	%
			18C6/SDS = 0.5			
150	3−5	88	80−120	12		
135	3−5	82	200−500	18		
90	3−5	81	120−200	19		
50	3−5	61	200−500	39		
			18C6/SDS = 1.0			
150	3−5	95	120−200	5		
135	3−5	90	200−500	10		
90	3−5	80	200−300	20		
50	3−5	76	300−800	24		
			18C6/SDS = 1.5			
150	3−5	73	300−500	27		
135	3−5	74	300−800	26		
90	3−5	77	300−500	23		
50	3−5	80			500−1200	20

light obtained by the CONTIN analysis for the three 18C6/SDS samples with ratios 0.5, 1.0, and 1.5 at 20 °C in the angular range 150−50°. With the exception of the largest ratio (1.5) and smallest angle (50°), large size aggregates are not observed. The dominant part of the scattered light is due to micelles, with the remaining contribution from midsize aggregates. The latter appears slightly increasing with 18C6/SDS ratio. The residuals are lower than 5% at ratio 0.5, and lower than 10% both at ratio 1.0 and 1.5.

The above results appear on the line of supporting the fact that the more ligands in the solution, the larger the CPMs, although on the basis of less pronounced evidence.

18C6 Samples at 30−40 °C. In Table 7, the light intensity distribution for the SDS sample with ratio 18C6/SDS = 1.0 is reported in the angular range 150−50° at different temperatures. The measurements have been performed after 1 night of stabilization at 30 and 40 °C and back at 20 °C with and without stirring. The contribution of the micelles is high for all temperatures. The medium CPMs are present at 30 °C in some amount, while at 40 and 20 °C with and without stirring they are almost negligible.

The residuals are lower than 8% at 30 °C, lower than 9% at 40 °C, lower than 10% at 20 °C without stirring, and lower than 9% at 20 °C with stirring.

Table 7. SDS Sample with Ratio 18C6/SDS = 1.0 in the Angular Range 150−50° at Different Temperatures

θ (angular deg)	micelles ø (nm)	%	aggreg medium (nm)	%	aggreg large (nm)	%
			At 30 °C			
150	3−5	50	800−1200	50		
135	3−5	58	800−1200	42		
90	3−5	100				
50	3−5	80	80	6	5000	23
30	3−5	66	50−80	7	2000−5000	27
			At 40 °C			
150	3−5	79	500−800	21		
135	3−5	91			5000	9
90	3−5	90			5000	10
60	3−5	72			5000	28
30	3	68			800−3000	32
			At 20 °C without Stirring			
150	3−5	86	300	6	3000−5000	8
135	3−5	97	800−1200	2	5000	1
90	3	100				
50	3−5	87			5000	13
30	3	68	200−300	7	3000−5000	25
			At 20 °C with Stirring			
150	3−5	82	300	4	3000−5000	14
135	3−5	80			3000−5000	20
90	3−5	88			5000	12
50	3−5	86			1200−5000	14
30	3	64	300−500	21	5000	15

Small Angle X-ray Scattering. Figure 6 reports the log−log plot of the SAXS curves at 20 °C for the SDS micellar solutions decorated by K222 (top panel) or 18C6 (bottom panel) with ligand/SDS ratios of 1.5, 1.0, and 0.5 in the full Q range accessed by the instrument. The present investigation extends and completes preliminary SANS studies performed on similar ligand−SDS micellar systems.[4,6,7] The case of SDS micellar solutions without any ligands was already reported in the literature.[7] Two regions can be clearly distinguished in Figure 6: at high Q, the curves show the presence of an interaction peak at about $Q = 0.2$ Å^{-1} due to the repulsion existing between the primary SDS micelles, whereas at low Q values the curves are dominated by the presence of CPMs as seen by the huge increase of scattered intensity.

SAXS curves have been fitted in the 0.15−0.30 Å^{-1} range to disclose the effect of the two ligands on the micellar structure. The CPM region has been analyzed using Guinier's approach.

The analysis of the micellar contribution to the SAXS curves (fits in Figures 7 and 8) was performed using a model where the particles are made of an inner core (the surfactant tails) and an outer layer (the polar head groups of the SDS surfactant). The assumed arrangement is that of a two-shell prolate ellipsoid. The normalized structure factor accounting for the shape of the micelles is the so-called form factor, $P(Q)$. The interparticle structure factor $S(Q)$ was calculated assuming an analytical solution based on the Hayter−Penfold model[24,25] considering a multicomponent ionic liquid in the mean spherical approximation. $S(Q)$ is the result of the hard-sphere repulsion and screened Coulomb repulsion between micelles. The multicomponent system was reduced to an effective one-component macroion system under the Gillan condition.[8]

Figures 7 and 8 show the detail of the interaction peak for the K222/SDS and 18C6/SDS, respectively. A small bump is
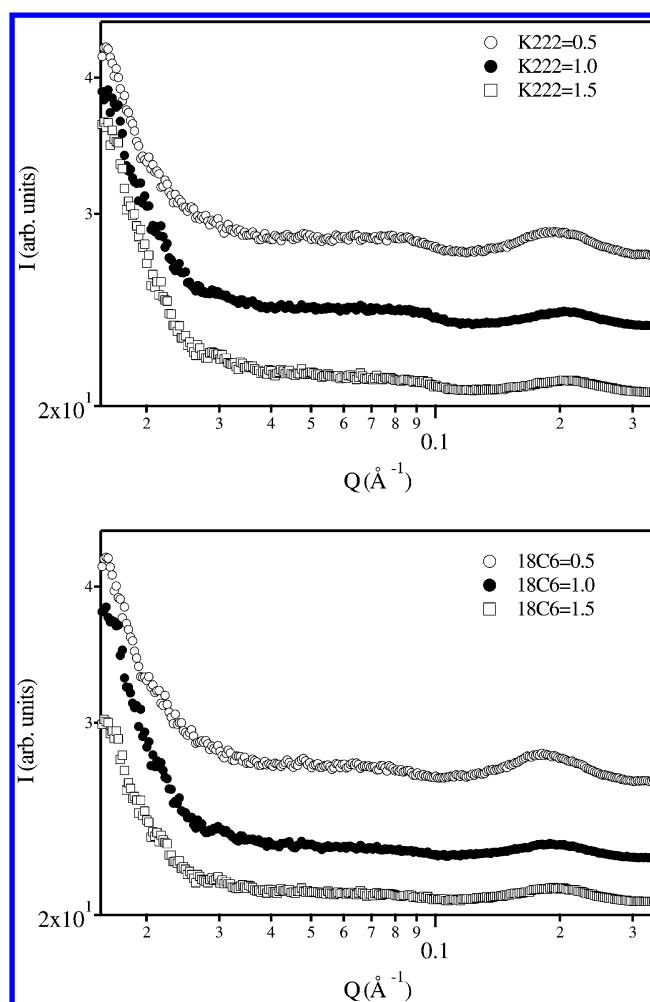

Figure 6. Log−log representation of the SAXS intensity distributions for K222/SDS micellar solutions (top panel) and 18C6/SDS micellar solutions (bottom panel) as a function of the ligand/SDS ratio. Original data have been offset for graphical purposes.
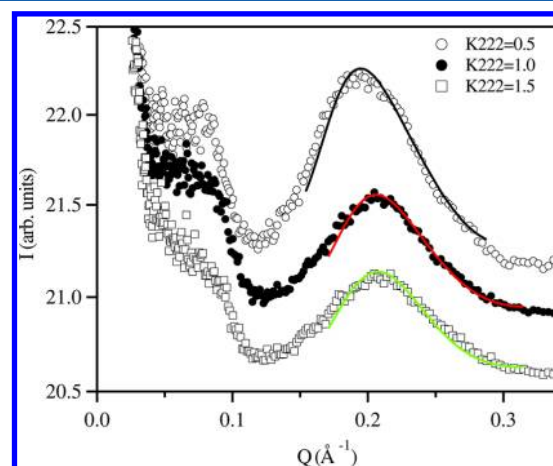

Figure 7. SAXS intensity distribution of SDS micellar solutions with K222 ratios of 0.5 (open circles), 1.0 (solid circles), and 1.5 (open squares). The fits of the micellar region (black, red, and green) are also shown (solid lines). Original data and the corresponding fitting have been offset for graphical purposes.

present in all cases at about $Q = 0.05$ Å^{-1} as a result of the superposition of the form factor $P(Q)$ proper of the SDS
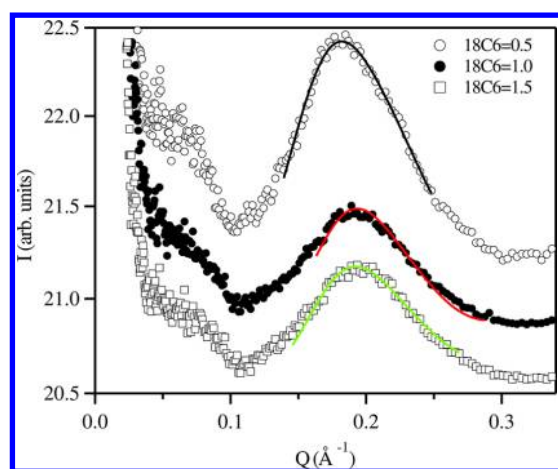
Figure 8. SAXS intensity distribution of SDS micellar solutions with 18C6 ratios of 10.5 (open circles), 1.0 (solid circles), and 1.5 (open squares). The fits of the micellar region (black, red, and green) are also shown (solid lines). Original data and the corresponding fitting have been offset for graphical purposes.

micelles[44] (which appears as hollow spheres to X-rays) with the CPM intensity increase dominating the low Q region of the SAXS curve.

The parameters characterizing the structure and interaction of the SDS micelles are the surface charge, Z, the average aggregation number, N, the shell thickness, t_h, the number of carbon atoms for a SDS monomer in the core, N_c, the percentage of the interfacial ligand molecules with respect to the total surfactant molecules, N_{lig}, the ellipsoidal axial ratio, a/b, the micellar diameter, d, the Debye length, D_{length}, the contact potential, V, and the volume fraction, vol$_{fract}$, of the surfactant present in the solution. The parameters extracted from the fitting were Z, N, t_h, N_{lig}, N_c, and the background. The latter quantity was estimated by the Porod analysis at high Q values.[45] a/b, d, Debye's length, V, the volume fraction, and the number N_s of water molecules for one surfactant molecule (hydration number) can be derived from the fitting outputs.

Table 8 lists the results obtained by the SAXS analysis of the micellar solutions with both ligands at ligand/SDS ratios of 1.5, 1.0, and 0.5. The errors on the fit parameters are reported as relative standard deviation.

In the case of the K222/SDS system increasing the ratio from 0.5 to 1.5, the parameters Z, N, N_c, diam, and V decrease while the parameters t_h, N_s, and vol$_{fract}$ remain constant and D_{length} increases. N_{lig} and a/b do not show a simple behavior. In the case of 18C6, the behavior of the fitting parameters is in general more various.

Comparing the SAXS data listed in Table 8 with previous SANS results,[4,6,7] it is clear that small angle scattering experiments are consistent in the three K222/SDS cases. Data for the 18C6/SDS sample with a ratio of 1.0 of Table 8 are in agreement with previous results obtained using SANS.[4,6]

The main effects imposed by the decoration of SDS micelles with adhesive sites are described in the following. On one hand, increasing the 18C6/SDS ratio, the shell thickness does not change from the value 5.5 Å obtained by SANS in the case of SDS micelles without ligands.[32] On the other hand, the micellar charge, Z, decreases both with respect to the "naked" case and increasing the ligand/SDS ratio. From these results, we can infer that the crown-ether ligands accommodate the crown parallel to the micellar surface and complex some sodium ion present in the Gouy−Chapman layer. The 18C6/SDS = 0.5 sample is similar to the sample where "naked" SDS micelles are considered.[22] In particular, at 0.250 M (which is close to our SDS concentration) and 25 °C, the reported results of Z = 26.7, N = 94.5, axial ratio 1.3, and D = 49.2 Å are very close to the values obtained in this work for the 18C6/SDS = 0.5 case.

Comparing with data obtained for hydrogenated 8 wt %/wt SDS micelles without K222,[32] we note that the effect of K222 addition to SDS micellar solution is to increase the outer layer thickness from 5.5 to 10−12 Å.[4] Furthermore, we observe again a decrease of the effective micellar charge from 30 to 10−20 and of the average aggregation number from 90 to 55−75.

As confirmed by the constant value of N_c for the three samples of the 18C6 series, the crown-ether is less effective than K222 to move to the micellar interface and does not enter into the micellar hard-core. A slight increase of N_{lig} is observed for the increase of the ligand/surfactant ratio. The micellar diameters for 18C6 are smaller than for K222 samples. The Debye length, volume fraction, and contact potential do not change as a function of the ratio, while N increases when the ratio decreases.

As a result of the addition of the ligand, a huge intensity increase is detected in the SAXS curves at low Q values, evidencing the presence of structures larger than the primary micelles, i.e., CPMs. This low Q region, not accessed previously by SANS measurements, can help in characterizing the aggregates of micelles. To this aim, we analyzed the data with Q below 0.025 using the Guinier law.[46] The plots of $\ln(I)$ as a function of Q^2 (i.e., Guinier's representation) are shown in Figures 9 and 10. The error bar for the data points is ±0.02 for K222 and ±0.03 for 18C6.

If $QR < 1$ (where R is the radius of a spherical scattering object), the Guinier equation holds

$$I(Q) = K^2 \text{Vol}^2 e^{-Q^2 R_g^2/3} \tag{4}$$

Table 8. Fitting Results according to a Prolate Ellipsoidal Core-Shell Form Factor Coupled with a Repulsion Potential for the Samples K222/SDS and 18C6/SDS with Ratios 1.5, 1.0, and 0.5 at 20 °C

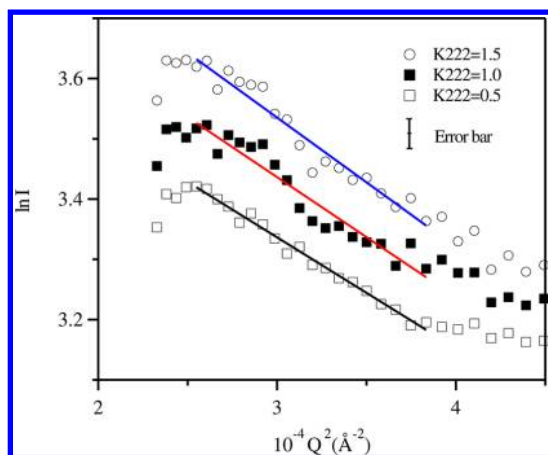|	Z	N	t (Å)	N_c	N_{lig} (%)	a/b	N_s	diam (Å)	D_{length} (Å)	V (k_BT)	vol frac
					K222/SDS						
1.5	12 ± 1	56 ± 8	11 ± 1	8.9 ± 1.8	59 ± 1	1.7	21	53	18	3.2	0.201
1	15 ± 1	59 ± 15	11 ± 4	8.9 ± 2.0	68 ± 10	1.8	21	54	17	4.1	0.211
0.5	21 ± 3	74 ± 13	10 ± 2	12 ± 0.4	40 ± 3	1.3	21	57	16	6.7	0.206
					18C6/SDS						
1.5	20 ± 3	84 ± 12	5.5 ± 1.0	12 ± 0.7	15 ± 3	1.5		50	17	9.7	0.115
1	27 ± 3	74 ± 5	5.5 ± 1.0	12 ± 1.1	12 ± 2	1.3		48	14	14	0.121
0.5	18 ± 2	103 ± 10	5.5 ± 0.7	12 ± 1.7	10 ± 1	1.85		52	19	8.2	0.116

Figure 9. Plots of Guinier's region (the smaller Q region) for CPMs with K222 ligand at 20 °C and ratios of 1.5 (open circles), 1.0 (solid squares), and 0.5 (open squares). The solid lines are the fit results. The error estimate on $\ln(I)$ is ±0.02. Original data and the corresponding fitting have been offset for graphical purposes.
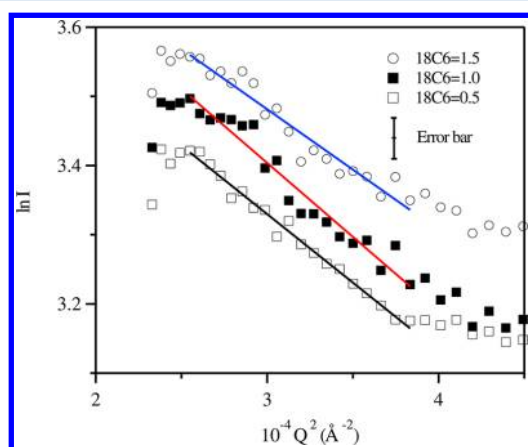

Figure 10. Plots of Guinier's region (the smaller Q region) for CPMs with 18C6 ligand at 20 °C and ratios of 1.5 (open circles), 1.0 (solid squares), and 0.5 (open squares). The solid lines are the fit results. The error estimate on $\ln(I)$ is ±0.03. Original data and the corresponding fitting have been offset for graphical purposes.

and data have a linear trend when $\ln I(Q)$ versus Q^2 is plotted; R_g is the gyration radius of the CPMs, K is a constant, and Vol is the particle's volume. R_g was then calculated from the slope of the straight lines in Figures 9 and 10 using in all cases 20 data points in the Q^2 region from 2.5×10^{-4} to 3.8×10^{-4} Å^{-2}. Assuming that the CPMs are spherical, the geometric radius R is related to the gyration radius by the equation $R = R_g(5/3)^{1/2}$. From this calculation, we extracted the average CPM radius reported in Table 9 for all the investigated cases.

As shown in Table 9, the CPM size is about 200 Å in the two distinct series. This value is quite small compared to the

Table 9. Radius of CPMs Decorated by the K222 or 18C6 Ligands[a]

K222/SDS	R (Å)	18C6/SDS	R (Å)
1.5	103	1.5	91.4
1.0	100	1.0	104
0.5	96.2	0.5	101

[a]The standard deviation on the calculated CPM size is below 10%.

dimensions of the CPMs obtained by DLS and is below the maximum dimension achievable by the present SAXS experiment (i.e., about 300 Å). By using the Guinier law, we see only the smaller CPMs present in the samples which could be responsible for the generation of the greater structures evidenced by DLS in the submicrometer/micrometer range. An ultra-SAXS experiment could be performed in the near future to cover a broader range of dimensions that superimpose to DLS and confirm this point.

■ DISCUSSION

The work reported in this paper was performed to investigate the aggregation process of micelles into CPMs in a solution of SDS micelles decorated with K222 or 18C6 ligands. CPMs of two main sizes were detected primarily in the submicrometer/micrometer range by DLS. Furthermore, we studied the stability and the reversibility of the system, considering that the nondecorated SDS micellar solutions do not aggregate.

The system of decorated micelles is characterized by a low amount of isolated micelles in solution, 8% w/w of solute (SDS), chosen with the aim to avoid aggregation between the "naked" micelles. The only perturbation imposed to the SDS micellar aqueous solution is the addition of the ligand which has the primary effect to decorate the micelles with adhesive sites. The amount of added K222 or 18C6 ligand maintains the sample homogeneous from 20 to 40 °C. SAXS results evidenced a different hydrophobic effect of the two ligands, being 18C6 less hydrophobically effective than K222 in agreement with previous SANS investigations.

In the SAXS curves, we could distinguish a micellar region at intermediate/high Q and a CPM region at low Q. The latter was useful to detect the smaller aggregates present in the CPMs by using the Guinier law. The maximum diameter of the observed CPMs is approximately 200 Å for all the SDS samples with K222 or 18C6 ligands, meaning that they are formed by about 50−100 micellar units. These entities can be the smaller clusters giving rise to the CPMs. An ultra-SAXS experiment covering a lower Q range is necessary to detect aggregates greater than 200−300 Å and confirm this hypothesis.

In Tables 3, 4, and 5, the DLS results by CONTIN analysis are reported for the micellar solutions with K222 ligand and in Tables 6 and 7 those with 18C6 ligand.

The study was performed at different times to explore the temporal evolution. Short and long time intervals were tested. The reported findings suggest that the decorated micellar solutions are fairly stable over a time interval of the order of 1 month. An experiment conducted on a sample at a time interval of 2 years appears to indicate that the stability is not fully maintained over such a long time.

■ CONCLUSION

Sodium dodecyl sulfate in water, decorated with various adhesive sites (Kryptofix 222 and 18-Crown-6), has been investigated by DLS and SAXS to study the micelle structure and interactions. Special attention was attracted by the formation of micelle aggregates, here named cluster phases of micelles, characterized by medium and large size in the submicrometer/micrometer range. As is well-known, the SDS micelles in water do not aggregate at the low surfactant concentration used in this paper; however, with respect to previous works and literature, we demonstrate that SDS micelles decorated with macrocyclic ligands do aggregate

depending on the ligand/surfactant molar ratio. The hydrophobicity of the adhesive sites (ligand molecules) and the complexation ability, greater for Kryptofix 222 than for 18-Crown-6, give rise to adhesive forces that induce the formation of CPMs. The sizes and the percentages of the micelles and the CPMs were studied at 20, 30, and 40 °C by DLS to test the stability and reversibility of the system, and at 20 °C by SAXS.

DLS results evidence that the CPM formation processes are fairly reproducible for both types of decorated micelles. At a given temperature, the more ligand is added to the micellar solution, the larger are the CPMs present in the samples. The Guinier analysis was used in the low Q region of the SAXS curves to obtain the sizes of the CPMs and the number of micelles for a given CPM. The results indicate that smaller CPMs are present in the solutions almost independently by the ligand used in this work.

■ AUTHOR INFORMATION

Corresponding Author
*E-mail: cecilia.gambi@fi.infn.it.

Notes
The authors declare no competing financial interest.

■ ACKNOWLEDGMENTS

■ REFERENCES

(1) Gokel, G. W. *Crown Ethers & Cryptands*; The Royal Society of Chemistry: Cambridge, U. K., 1994.

(2) Hunter, R. J. *Foundations of Colloid Science*; Oxford Science Publications, Clarendon Press: Oxford, U. K., 1987; Vol. *1*.

(3) Evans, D. F.; Wennestrom, H. *The Colloidal Domain Where Physics, Chemistry, Biology, and Technology Meet*; VCH Publishers, Inc.: New York, 1994; Chapter 1, pp 8−9.

(4) Baglioni, P.; Gambi, C. M. C.; Giordano, R.; Teixeira, J. The Role of Macrocyclic Ligands on the Structure of LDS Micellar Solutions. *Physica B* **1995**, *213 & 214*, 597−599.

(5) Carlà, M.; Gambi, C. M. C.; Baglioni, P. Adsorption Properties of Cryptand 222 at the Charged Mercury-Solution Interface. *J. Phys. Chem.* **1996**, *100*, 11067−11071.

(6) Baglioni, P.; Gambi, C. M. C.; Giordano, R.; Teixeira, J. Complexation of Counterions in Micellar Solutions: A Small Angle Neutron Scattering Study. *Colloids Surf., A* **1997**, *121*, 47−52.

(7) Scaffei, L.; Lanzi, L.; Gambi, C. M. C.; Giordano, R.; Baglioni, P.; Teixeira, J. Study by Small-Angle Neutron Scattering of Sodium Dodecyl Sulfate Micelles with the Macrocyclic Ligand [2.2.2.]-Cryptand. *J. Phys. Chem. B* **2002**, *106*, 10771−10776.

(8) Gillan, M. A Simple Model for the Classical One-Component Plasma. *J. Phys. C* **1974**, *7*, L1−L4.

(9) Bianchi, E.; Largo, J.; Tartaglia, P.; Zaccarelli, E.; Sciortino, F. Phase Diagram of Patchy Colloids: Towards Empty Liquids. *Phys. Rev. Lett.* **2006**, *97*, 168301-1−168301-4.

(10) Cardinaux, F.; Stradner, A.; Schurtenberger, P.; Sciortino, F.; Zaccarelli, E. Modeling Equilibrium Clusters in Lysozyme Solutions. *EPL* **2007**, *77*, 48004-p1−48004-p5.

(11) Lonetti, B.; Fratini, E.; Chen, S.; Baglioni, P. Viscoelastic and Small Angle Neutron Scattering Studies of Concentrated Protein Solutions. *Phys. Chem. Chem. Phys.* **2004**, *6*, 1388−1395.

(12) Liu, Y.; Fratini, E.; Baglioni, P.; Chen, W.-R.; Chen, S.-H. Effective Long-Range Attraction between Protein Molecules in Solutions Studied by Small Angle Neutron Scattering. *Phys. Rev. Lett.* **2005**, *95* (11), 118102-1−118102-4.

(13) Porcar, L.; Falus, P.; Chen, W.-R.; Faraone, A.; Fratini, E.; Hong, K.; Baglioni, P.; Liu, Y. Formation of the Dynamic Clusters in Concentrated Lysozyme Protein Solutions. *J. Phys. Chem. Lett.* **2010**, *1*, 126−129.

(14) Liu, Y.; Porcar, L.; Chen, J.; Chen, W.-R.; Falus, P.; Faraone, A.; Fratini, E.; Hong, K.; Baglioni, P. Lysozyme Protein Solution with an Intermediate Range Order Structure. *J. Phys. Chem. B* **2011**, *115*, 7238−7247.

(15) Baglioni, P.; Fratini, E.; Lonetti, B.; Chen, S. H. Structural Arrest in Concentrated Cytochrome C Solutions: the Effect of pH and Salts. *J. Phys.: Condens. Matter* **2004**, *16*, S5003−S5022.

(16) Stradner, A.; Sedgwick, H.; Cardinaux, F.; Poon, W.; Egelhaaf, S.; Schurterberger, P. Equilibrium Cluster Formation in Concentrated Protein Solutions and Colloids. *Nature* **2004**, *432*, 492−495.

(17) Campbell, A.; Anderson, V. J.; van Duijneveldt, J.; Bartlett, P. Dynamical Arrest in Attractive Colloids: the Effect of Long-Range Repulsion. *Phys. Rev. Lett.* **2005**, *94*, 208301-1−208301-4.

(18) Sciortino, F.; Mossa, S.; Zaccarelli, E.; Tartaglia, P. Equilibrium Cluster Phases and Low-Density Arrested Disordered States: the Role of Short-Range Attraction and Long-Range Repulsion. *Phys. Rev. Lett.* **2004**, *93*, 055701-1−055701-4.

(19) Segré, P.; Prasad, V.; Schofield, A.; Weitz, D. Glasslike Kinetic Arrest at the Colloidal Gelation Transition. *Phys. Rev. Lett.* **2001**, *86*, 6042−6045.

(20) Dinsmore, A.; Weitz, D. Direct Imaging of Three-Dimensional Structure and Topology of Colloidal Gels. *J. Phys.: Condens. Matter* **2002**, *14*, 7581−7597.

(21) Sedgwick, H.; Egelhaaf, S.; Poon, W. Clusters and Gels in Systems of Sticky Particles. *J. Phys.: Condens. Matter* **2004**, *16*, S4913−S4922.

(22) Payne, K.; Magid, L.; Evans, D. Structural Changes in Anionic Micelles Induced by Counterion Complexation with a Macrocyclic Ligand: A Neutron Scattering Study. *Prog. Colloid Polym. Sci.* **1987**, *73*, 10−17.

(23) Caponetti, E.; Chillura Martino, D.; Floriano, M.; Triolo, R. Application of the Small-Angle Neutron Scattering Technique to the Study of Solubilization Mechanisms of Organic Molecules by Micellar Systems. *Mol. Struct.* **1996**, *383*, 133−143.

(24) Hayter, J.; Penfold, J. An Analytic Structure Factor for Macro-Ion Solutions. *J. Mol. Phys.* **1981**, *42*, 109−118.

(25) Hayter, J. Concentrated Colloidal Dispersions Viewed as One-Component Macrofluids. *Faraday Discuss. Chem. Soc.* **1983**, *76*, 7−17.

(26) Bendedouch, D.; Chen, S.-H.; Koehler, W. Structure of Ionic Micelles from Small Angle Neutron Scattering. *J. Phys. Chem.* **1983**, *87*, 153−159.

(27) Chao, Y.; Sheu, E. Y.; Chen, S.-H. Experimental Test of a Theory of Dressed Micelles: the Case of Monovalent Counterion. *J. Phys. Chem.* **1985**, *89* (22), 4862−4866.

(28) Brown, W. *Dynamic Light Scattering - The Method and some Applications*; Oxford Science Publications: Oxford, U.K., 1993; p 177.

(29) Lanzi, L.; Carlà, M.; Lanzi, L.; Gambi, C. M. C. Dielectric Spectroscopy by Differential Measurements in Transmission Lines on Sodium Dodecyl Sulfate Micelles in Water. *J. Non-Cryst. Solids* **2005**, *351*, 2864−2867.

(30) Lanzi, L.; Carlà, M.; Lanzi, L.; Gambi, C. M. C. A New Insight on the Dynamics of Sodium Dodecyl Sulfate Aqueous Micellar Solutions by Dielectric Spectroscopy. *J. Colloid Interface Sci.* **2009**, *330* (1), 156−162.

(31) Sennato, S.; Marchetti, S.; Gambi, C. M. C.; Cametti, C. Complexation of Macrocyclic Ligands in Ionic SDS Micellar Solutions: A Dielectric Spectroscopy Investigation. *J. Non-Cryst. Solids* **2011**, *357* (2), 754−759.

(32) Grosse, C. In *Encyclopedia of Surface and Colloid Science*; Hubbard, A. T., Ed.; Dekker: New York, 2002.

(33) Cazzolli, G.; Caponi, S.; Defant, A.; Gambi, C. M. C.; Marchetti, S.; Mattarelli, M.; Montagna, M.; Rossi, B.; Rossi, F.; Viliani, G.

Aggregation Processes in Micellar Solutions: a Raman Study. *J. Raman Spectrosc.* **2012**, *43*, 1877−1883.

(34) Evans, D.; Ser, R.; Warr, G. Structural Changes in Sodium Dodecyl Sulfate Micelles Induced by Using Counterion Complexation by Macrocyclic Ligands. *J. Phys. Chem.* **1986**, *90*, 5500−5502.

(35) Evans, D.; Evans, J.; Sen, R.; Warr, G. A Comparison of Counterion Effects in Surfactant and Classical Colloid Systems. *J. Phys. Chem.* **1988**, *92*, 784−790.

(36) Selassie, C. *History of Quantitative Structure-Activity Relationships*; Wiley: New York, 2003; Vol. Burger's Medicinal Chemistry and Drug Discovery, Chapter 1.

(37) Cambridge Software, http://www.cambridgesoft.com.

(38) Crippen, N. Atomic Physicochemical Parameters for Three-Dimensional-Structure-Directed Quantitative Structure-Activity Relationships. 2. Modeling Dispersive and Hydrophobic Interactions. *J. Chem. Inf. Comput. Sci.* **1987**, *27* (1), 21−35.

(39) Broto, P.; Moreau, G.; Vandycke, C. Molecular Structures: Perception, Autocorrelation Descriptor and SAR Studies. *Eur. J. Med. Chem.* **1984**, *19*, 71−78.

(40) Berne, B. J.; Pecora, R. *Dynamic Light Scattering*; Dover: New York, 2000.

(41) Provencher, S. A Constrained Regularization Method for Inverting Data Represented by Linear Algebraic or Integral Equations. *Comput. Phys. Commun.* **1982**, *27*, 213−227.

(42) Blanton, T.; Huang, T.; Toraya, C., H.; Hubbard; Robie, S.; Louer, D.; Gobel, H.; Will, G.; Gilles, R.; Raftery, T. JCPDS - International Centre for Diffraction Data Round Robin Study of Silver Behenate. A Possible Low-Angle X-ray Diffraction Calibration Standard. *Powder Diffr.* **1995**, *10*, 91−95.

(43) Ilavsky, J.; Jemian, P. Irena: Tool Suite for Modeling and Analysis of Small-Angle Scattering. *J. Appl. Crystallogr.* **2009**, *42* (2), 347−353.

(44) Zemb, T.; Charpin, P. Micellar Structure from Comparison of X-ray and Neutron Small-Angle Scattering. *J. Phys. (Paris)* **1985**, *46*, 249−256.

(45) Auvray, L.; Auroy, P. *Neutron, X-Ray and Light Scattering*; North Holland: Amsterdam, 1991; Chapter 3, pp 199−221.

(46) Guinier, A.; Fournet, G. *Small-Angle Scattering of X-rays*; John Wiley & Sons, Inc.: New York, 1955.